DOI: 10.1002/stco.202500025

Pauline Markreiter, Adrian Münch, Imke Engelhardt, Philipp Weidner, Thomas Ummenhofer

ARTICLE

Numerical investigations of T-joints made of high-strength square hollow sections

This article presents the results of numerical investigations of T-joints made of high-strength square hollow sections under axial and bending loads. The work builds on the experimental results of FOSTA project P1504 by using detailed finite element modelling. These models were validated against test results and include a calibrated break-off criterion that represents punching shear failure. Systematic parameter studies examined the effects of steel grade, the β-ratio, chord wall thickness, weld geometry and chord pre-stressing. The results confirm that, for β-ratios between 0.4 and 0.7, the current Eurocode design rules (prEN 1993-1-8) are conservative, even without the material reduction factor C_f. However, for larger β-ratios and thicker chord walls, the design rules tend to overestimate the load-bearing capacity of the joints. For bending, tensile pre-stressing improves resistance, which is underestimated by the current standard. The study suggests that adjusting the chord stress functions and including weld effects and effective width ratios could improve the accuracy and efficiency of designing joints for high-strength hollow section structures.

Keywords high-strength steel; square hollow sections; T-joints; finite element analysis; punching shear failure; chord pre-stressing; parameter study

1 Introduction

Hollow section joints play a central role in large-span structures such as trusses, offshore structures or crane systems. The use of high-strength steels (e.g., S700MH, S890QH) opens up new potential for reducing cross-sectional dimensions and weight, which can reduce CO_2 emissions in particular. For the use of high-strength hollow sections according to DIN EN 10219-3 [1] and DIN EN 10210-3 [2], the previous design approaches according to the new draft of Eurocode 3 Part 1-8 (prEN 1993-1-8 [3]) are applicable up to and including steel grade S700. However, the introduction of general reduction factors, such as the material factor C_f, does not lead to efficient design due to conservative design approaches which had to be established due to a lack of knowledge and database from experimental and numerical investigations and significantly limits the advantage of the resource-saving use of high-strength hollow sections.

An increase in steel strength does not necessarily lead to a proportional increase in joint load-bearing capacity. In fact, the plastic deformation capacity of high-strength steels is reduced compared to usual steel grades, which is particularly critical in the case of high local strains in the joint area due to local effects. In addition, the influence of chord pre-stressing on the load-bearing capacity of high-strength hollow section joints has hardly been investigated to now.

As part of the research project P1504 [4] of the Research Association for Steel Application (FOSTA), welded T-joints made of high-strength hollow sections were experimentally investigated [5]. Two different types of loading conditions were considered: on the one hand, axially stressed T-joints, where tests were carried out at the Karlsruhe Institute of Technology (KIT) and on the other hand, bending stressed T-joints, where experimental investigation was carried out at the Munich University of Applied Sciences. The aim of the project was to systematically determine the load-bearing behaviour of high-strength T-joints under different load cases, geometries and steel grades and to critically question the suitability of existing design approaches and the necessity of the material factor C_f. More details are presented in [5].

This article represents the numerical extension of the experimental investigations. Based on the experimental data obtained in project P1504 [4], detailed finite element models (FEMs) were developed and validated. Analogous to the experimental implementation, numerical parameter studies were carried out separately for each loading type at the two research institutions. The objective of the investigations was to identify the decisive influencing variables on the load-bearing behaviour by systematically varying the geometric parameters and material boundary conditions as well as the chord pre-stressing and to derive data for the further development of existing design models.

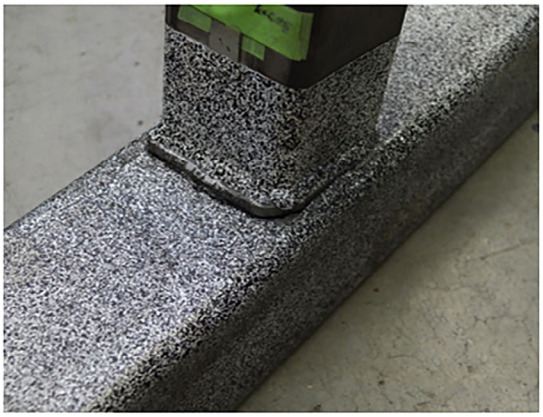

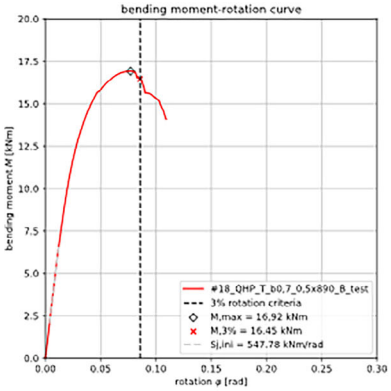

Fig. 1 PSF of a T-joint subjected to bending before reaching 3 % indentation [4]

2 Model development

In order to investigate the influence of various parameters on the joint load-bearing capacity of high-strength T-joints, it is necessary to supplement the experimental load-bearing tests with a numerical parameter study. This requires a validated FEM. The numerical investigations of the axially loaded T-joints were carried out using *ANSYS* Workbench 2023 R2 software. The numerical investigations of the T-joints subjected to bending stress were carried out using ABAQUS software. All tests were simulated to validate the FEMs. The validation of an FEM is always an iterative process in which the most favourable and sufficiently accurate discretisation must be selected, considering the computational effort, in order to carry out the parameter study efficiently.

Some of the test results show punching shear failure (PSF) mechanism (see Fig. 1). The FEM must therefore be able to represent this failure mechanism. In previous research projects (e.g., in [6, 7]), PSF was mostly neglected in the numerical simulation and the numerical results were evaluated using the $0.03 \cdot b_0$ deformation criterion according to Lu et al. [8]. Due to the fact that some tests have shown that an indentation of the brace into the chord of 3 % was not achieved before failure (see Fig. 1), this evaluation procedure is not appropriate for the numerical simulation of high-strength T-joints. Modelling of the local failure behaviour is possible in numerical simulation using material-dependent damage models [9]. The consideration of damage mechanisms in simulations requires the use of a calibrated damage mechanics model. The calibration of such models is associated with a very high experimental effort as well as in-depth knowledge in dealing with sensitivities regarding the mesh dependency. Within these investigations, a plastic material model was used for the numerical parameter studies. However, in order to be able to appropriately model the PSF mechanism, a break-off criterion was defined, at which the load-bearing capacity of the hollow section joint is numerically reached. The break-off criterion is based on the 'plastic damage' model according to Johnson and Cook [10, 11] and defines a plastic limit value dependent on triaxiality. As soon as this limit plastic strain is exceeded in one of the elements, the simulation is aborted. As a result, damage initiation and damage evolution, which could be considered when using a sophisticated damage mechanics model, are neglected. The determination of the triaxiality-dependent plastic limit strains for the materials used is described in [12]. The calibration and validation of the break-off criterion are carried out by comparison with the local failure behaviour in the experimental results. The following description of the model development is based on the example of axially stressed T-joints. The modelling of the T-joints supposed to bending is carried out analogously, but in the ABAQUS program environment.

2.1 Material modelling

The material model for input into an FE program is derived from the results of the tensile tests carried out in [4]. The linear elastic range is described by the modulus of elasticity for steel of 210,000 N/mm^2 and Hook's law. The plastic material behaviour is represented by a multilinear material model. For this purpose, the combined approach (linear ratio factor α) of the material models of Voce [13] and Swift [14] is used. This approach has often been successfully used in the literature to describe the damage behaviour of high-strength steels [15–17]. The parameters of the Voce and Swift material models for the steels used in this project were determined numerically using a fitting algorithm and can be found in Tab. 1.

2.2 Boundary conditions

The boundary conditions of the FEM were derived from the support conditions of the component tests (Fig. 2). The load in the vertical brace was applied

Tab. 1 Parameters of the material models according to Voce and Swift

Steel grade	Voce			Swift			
	A [−]	ε_0 [10^{-3}]	N [10^{-3}]	K_0 [−]	Q [−]	B [−]	A [−]
S700MH (SHS)	1200.50	33.19	117.81	806.61	184.43	13.23	0.65
S890QH (SHS)	1351.63	5.06	76.60	943.87	200.72	23.53	0.50

displacement-controlled and the force reaction of the boundary conditions was evaluated as the brace force.

As with the bolted joints in the component tests, the ends of the T-joint were hinged, with the directions of displacement locked in accordance with the static system. The vertical supports were modelled on the lower side of the chord with the corresponding support distance l_A.

For the models with chord pre-stressing, the numerical simulation was carried out, analogous to the component tests, in two steps. In the first simulation step, the brace was not supported, the pre-stress was applied and the displacements in the longitudinal direction of the chord at the brace support were saved as parameters. In the second simulation step, the parameters stored in the first step were used to displace the brace bearing accordingly. In the second load step, the displacement of the brace was blocked according to the static system and the load was applied in a displacement-controlled manner.

The symmetry of the T-joint was used to reduce the Central Processing Unit (CPU) time. The plane of symmetry is spanned by the longitudinal axes of the brace and the chord. The degree of freedom of translation in the x-direction was blocked for the nodes lying in the plane of symmetry. Due to the asymmetrical load and the pre-stressing, only one plane of symmetry could be used.

2.3 Discretisation

The hollow section joints were meshed using quadratic function elements. Adding Gaussian points to the elements (Solid-186 and Solid-187) with a quadratic function led to convergence in the simulations, with an element edge length of 2 mm and two elements over the wall thickness. Since calculated plastic strains depend on mesh size and the break-off criterion depends on plastic strain, all test specimens in the validation, recalculation and parameter study of the joint area were meshed with two-millimetre-edge-length elements.

2.4 Instrumentation

The chord indentation was determined in the FEM analogous to the measurement on the test specimen. The chord indentation is determined using the relative displacement of the two measuring points MPA and MPB (Fig. 3a).

To determine the stress state in the numerical model, evaluation paths were defined (Fig. 3b) at the locations where strain gauges were applied in the experimental investigations, in order to evaluate the normal stress in the strain gauges' measurement direction. The length of the evaluation paths corresponds to the measuring grid length of the strain gauges.

2.5 Geometry modelling

To validate the numerical models, the test specimens were optically measured using a CREAFORM HandySCAN 3D handheld laser. The optical measurement allows to record manufacturing imperfections such as deviations in the brace angle and profile dimensions as well as the exact geometry of the weld. The surface geometry from the laser scan was converted into a 3D CAD model (see Fig. 4). Numerical comparative calculations in [4] have shown that modelling the T-joints with a simple substitute geometry

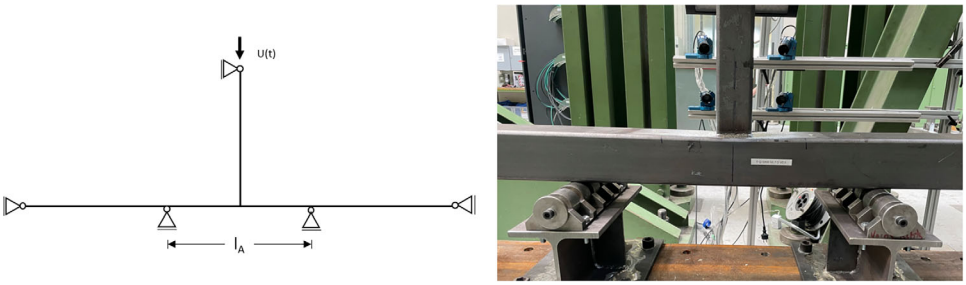

Fig. 2 Static system derived from the support conditions of the component tests

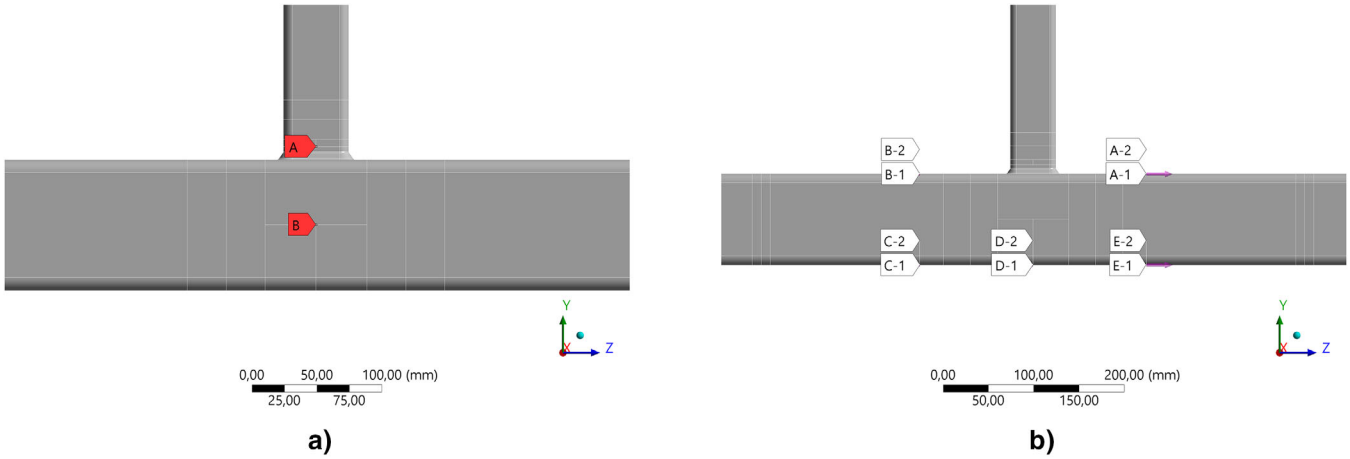

Fig. 3 Position of measuring points a) MPA and b) MPB evaluation paths of the strain gauges [4]

provides only minor deviations from the results with the scanned geometries, but that enormous computing time can be saved due to neglect of the discretisation of the real weld seam geometry. Therefore, the laser scans were only used to determine the weld seam dimensions and based on this, a substitute geometry was used to model the weld seam.

All other geometric dimensions such as height, width and wall thicknesses were determined manually using suitable measuring methods with calipers and micrometres. In particular, when measuring the wall thickness of the hot-finished square hollow sections, an increase in the wall thickness in the direction of the fillet radii was observed. This effect has a significant influence on the joint load-bearing capacity depending on the β-ratio. In addition, it has an effect on deviations in the numerical validation due to the constant modelling of the wall thicknesses with the corresponding normative fillet radii in the FE simulation. In order to take this effect into account, the influence of the radii on the chord plate thickness t_0 was considered by a flat-rate allowance of 50 %. This allowed the moment–rotation curve of the test to be mapped well within the FE calculation (see Fig. 5). In contrast, the wall thicknesses of the cold-formed hollow sections were found to vary only slightly due to the manufacturing process using thermo-mechanical rolled sheet metal. The wall thicknesses of the cold-formed hollow sections are generally below the normative specifications, but above the permissible tolerances according to DIN EN 10219-1 [18].

The geometries of the hollow section joints for the parameter study were modelled without a production-related attached fillet weld. The influence of the attached fillet weld on the joint load-bearing capacity was investigated numerically in a parameter study.

2.6 Break-off criterion

As already explained in Section 1, a break-off criterion is required in the numerical recalculation of the tests, which describes the beginning of the PSF with sufficient accuracy. In contrast to the use of a damage-mechanical material model, an engineering approach was chosen for this project, considering relevant influencing factors. According to the literature (e.g., [19]), the damage initiation strain or the critical plastic strain of the steel material depends on the existing stress state (triaxiality T). Experimental investigations on notched tensile specimens in [12] have shown that multiaxial tensile stresses ($T > 0.3$) in particular represent critical stress states. Numerical preliminary simulations on T-joints have shown that in the area of the weld seam transition, where the PSF could be observed in the tests, stress multiaxialities are present with values from $T = 0.3$ to $T = 0.8$ (see Fig. 6).

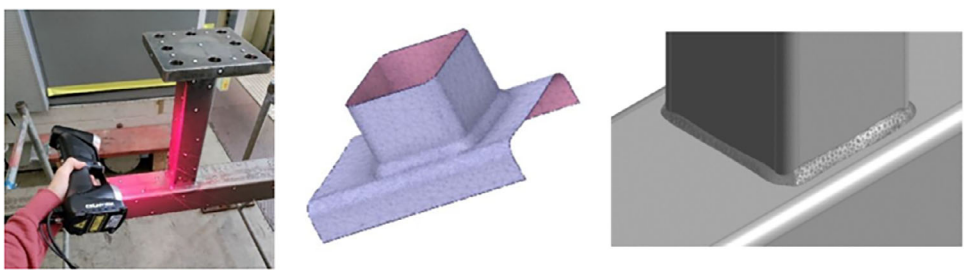

Fig. 4 Scanning process of the T-joints and transfer to a 3D CAD model

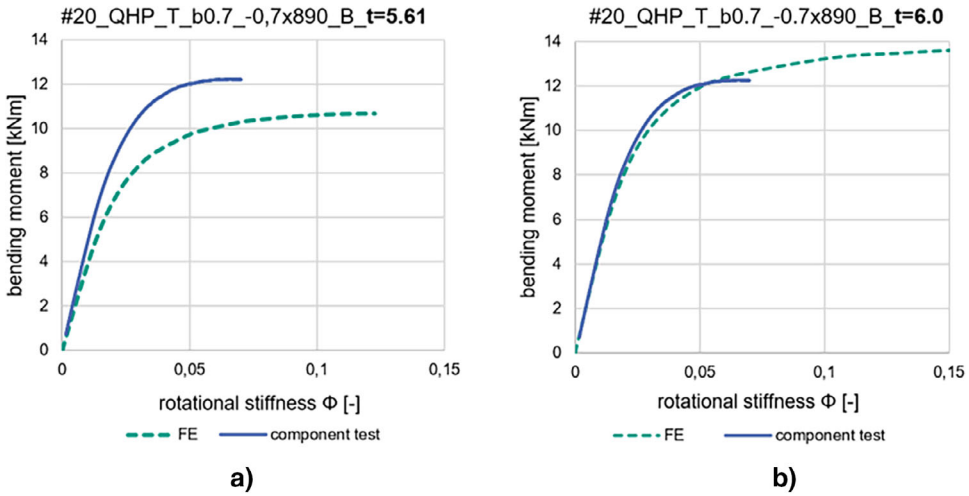

Fig. 5 Calibration of numerical simulation model on real component test #20: a) chord thickness t_0 measured in the centre and b) chord thickness t_0 with 50 % radius influence

In the numerical models of the T-joints subjected to axial tension, the load was applied displacement-controlled in a large number of load steps. At the end of each load step, a check was performed if the plastic strain, depending on the triaxiality, exceeds the critical strain according to the damage curve given in [12]. The calculation was terminated as soon as the damage initiation strain dependent on the stress multiaxiality was reached in a finite element. Although this pragmatic approach does not map the material damage (damage initiation and damage evolution) in detail, very good results were obtained for the recalculation of the component tests with regard to the maximum joint load-bearing capacity (see Fig. 9).

The 'ductile damage' module was used for the ABAQUS program environment for the load type bending. This can be used to realistically simulate ductile materials that fail due to plastic deformation before fracture. The model comprises three phases: (1) damage initiation at critical strain or stress, (2) progressive damage with decreasing stiffness and (3) complete failure when the 'displacement at failure' limit value is exceeded. This describes the maximum strain at which a damaged element is removed from the calculation. This value is used in combination with parameters such as elongation at failure and damage criteria to precisely map the material behaviour. The limit value selected for the 'displacement at failure' was determined iteratively and depends on the material. For example, a limit value of 0.15 was selected for steel grade S700MH, while the limit value for steel grade S890QHL was set at 0.1 (see Fig. 7).

2.7 Numerical comparative simulations

In the following, the validation of the numerical models is evaluated using the results of numerical comparative simulations. The numerical models were generated in accordance with the modelling development described in Sections 2.1–2.6. The results of the numerical comparative simulations are shown in Figs. 8 and 9 as examples. The force–indentation curves show good agreement between the numerical simulations and the experimentally determined curves, regardless of the steel grade, the β-ratio, the degree of pre-stressing and the direction of loading. Furthermore, the comparisons of the strain gauge measurements with the evaluations of the normal stresses

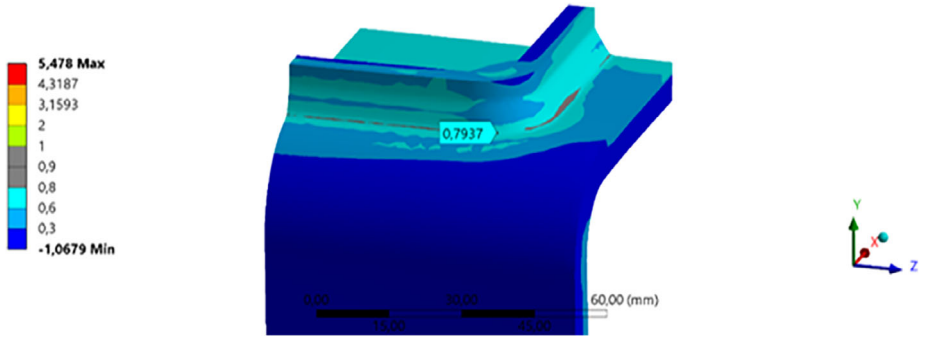

Fig. 6 Plot of triaxiality from numerical simulation of a T-joint subjected to axial tension

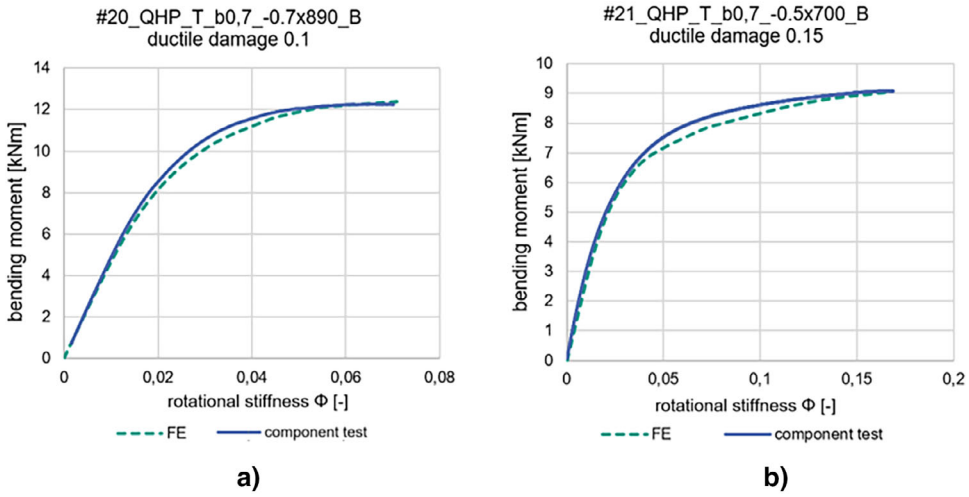

Fig. 7 Definition of limit value 'displacement at failure': a) #20_QHP_T_b0,7_-0,7x890_B_ductile damage 0.1 and b) #21_QHP_T_b0.7_-0.5x700_B_ductile damage 0.15

in the FEM also show good agreement. Based on these numerical comparative calculations, the numerical model and the break-off criterion used can be considered as validated.

3 Parameter studies

In the parameter study, the influences of various parameters on the load-bearing behaviour of high-strength T-joints made of square hollow sections were investigated numerically. The following section differentiates between two types of loading: T-joints subjected to bending and T-joints subjected to axial loading. The investigations included a large number of influencing variables, comprising the width ratio β, the degree of pre-stressing n of the chord, the chord slenderness 2γ and different high-strength steel grades. Tab. 2 provides an overview of all joint configurations considered (chord width × chord wall thickness _ brace width × brace thickness).

3.1 Axially loaded T-joints

The tests carried out in [4] have shown that T-joints subjected to axial tension always show a higher load-bearing capacity than T-joints subjected to axial compression. Since prEN 1993-1-8 [3] does not differentiate in the direction of loading, only a parameter study is carried out for the less favourable case, the brace subjected to axial compression. Fig. 10 shows the decisive failure mechanism according to prEN 1993-1-8 [3] as a function of the ratios 2γ and β. Fig. 10 shows that for the selected parameter range (area marked in red) of the numerical parameter study, the failure mechanism chord face failure (CFF) is always decisive. The $0.03b_0$ deformation criterion according to [8] is therefore used to evaluate the joint load-bearing capacities in the parameter study.

The following results are used to evaluate the design formula specified in prEN 1993-1-8 [3]. For this purpose,

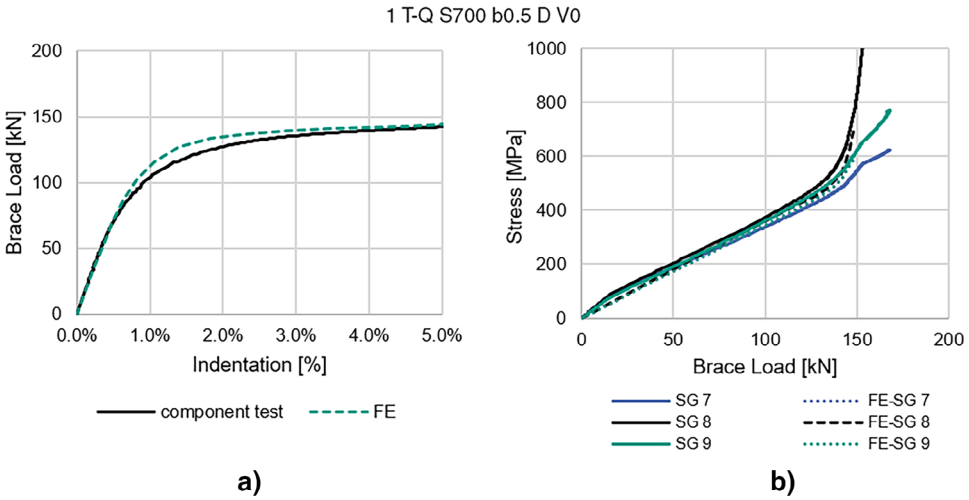

Fig. 8 Results of the numerical comparative calculation of test 1 T-Q S700 b0.5 D V0: a) force–indentation curve and b) comparison of the stress state

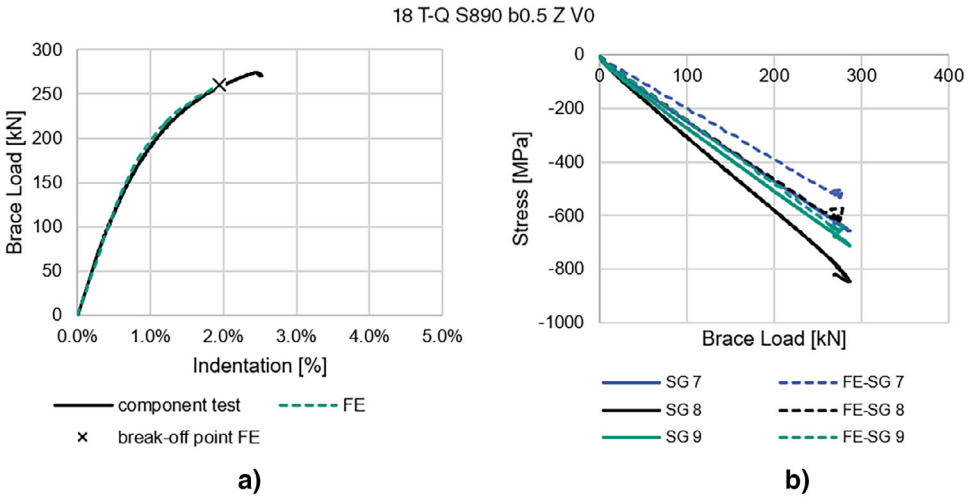

Fig. 9 Results of the numerical comparative calculation of test 18 T-Q S890 b0.5 Z V0: a) brace load–indentation curve and b) comparison of the stress state

Tab. 2 Selected parameter range for the numerical parameter study

2γ	Degree of preload n	β-ratio $\beta = b_1/b_0$					
		0.4		0.6		0.8	
		S700MH	S890QHL	S700MH	S890QHL	S700MH	S890QHL
20	−0.7; −0.5; 0; 0.5; 0.7	100 × 5.0_40 × 4.0		100 × 5.0_60 × 4.0		100 × 5.0_80 × 4.0	
17.5	−0.7; −0.5; 0; 0.5; 0.7	140 × 8.0_56 × 6.4		140 × 8.0_84 × 6.4		140 × 8.0_112 × 6.4	
14.4	−0.7; −0.5; 0; 0.5; 0.7	180 × 12.5_72 × 10.0		180 × 12.5_108 × 10.0		180 × 12.5_144 × 10.0	

the numerically determined joint load-bearing capacities r_n are compared with the theoretical joint load-bearing capacities r_t according to prEN. Since the input values (geometric dimensions and material properties) and the numerical results provide unambiguous measurement results, the statistical evaluation according to EN1990 Annex D is omitted. The diagrams in Fig. 11 show the coefficient of variation V_δ and the gradient of the mean value line b. If the mean value line lies above the straight line $r_n = r_t$, the mean value of all results lies above the theoretical joint load-bearing capacities of the prEN and is therefore conservative. The diagram in Fig. 11a shows the results of the calculation of the theoretical joint load-bearing capacity according to prEN 1993-1-8 [3] with a C_f factor of 0.8, as specified in the standard. Fig. 11b shows the results of the theoretical joint load-bearing capacity according to prEN 1993-1-8 [3] with a C_f factor of 1.0. Both diagrams show that the regression line of the mean value of all results lies above the straight line $r_t = r_n$.

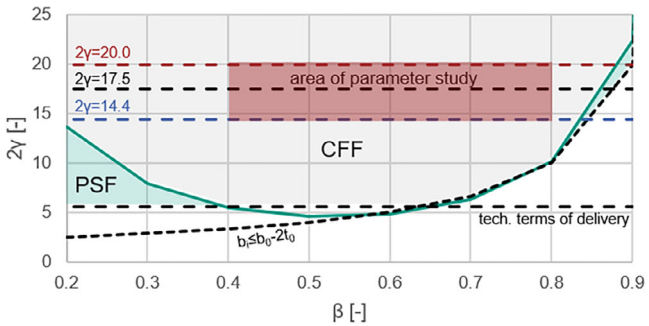

Fig. 10 Decisive failure mechanism for axially loaded T-joints according to prEN 1993-1-8 [3] as a function of the 2γ- and β-ratio

The diagrams also show a large coefficient of variation with $V_\delta > 0.2$. The results are very scattered, especially for high load-bearing capacities, which correlate with large β-ratios. From this it can be concluded that the yield line model used for the CFF mechanism is rather unsuitable for large β-ratios, as the load transfer mainly takes place via the side walls. Fig. 11b shows that an additional reduction of the joint load-bearing capacity of high-strength axially loaded T-joints by a C_f factor is not necessary. According to the available range of the numerical parameter study and experimental investigations, this statement is only valid for β-ratios of 0.4–0.7.

3.1.1 Influences on the load-bearing behaviour: axial

In the following, the influences of the investigated parameters are evaluated individually and compared with the design formulas of prEN 1993-1-8 [3] (Eq. (1)). On the one hand, charts are shown in which the results are related to a reference value. This representation has the advantage that the influence of the parameter under investigation

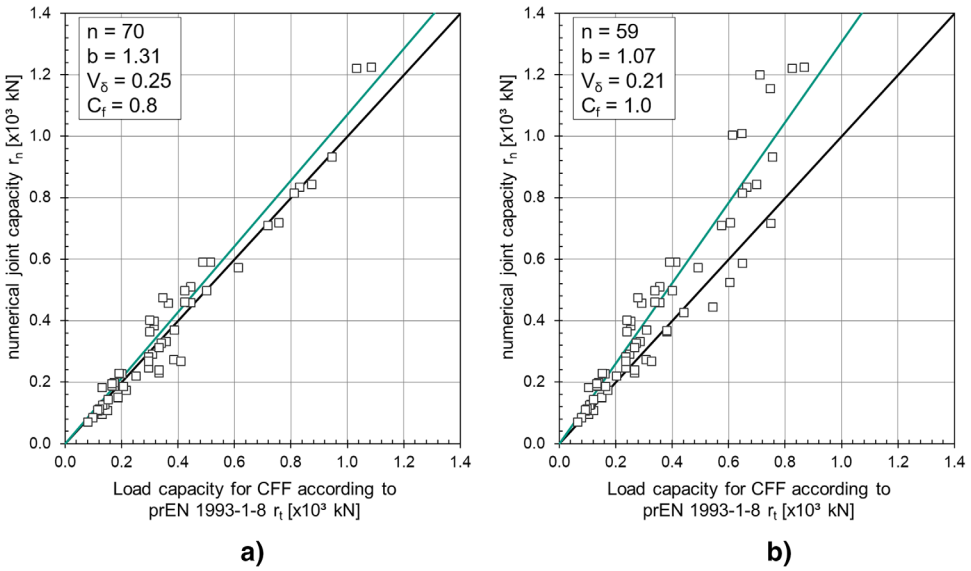

Fig. 11 Comparison of the numerically determined joint load-bearing capacities with the joint load-bearing capacities calculated according to prEN 1993-1-8 [3] a) using Cf-factor 0.8, b) using Cf-factor 1.0

can be shown separately, i.e., independently of the other influences. However, this representation is dependent on the selected reference point. A comparison of the shape of the normative curve and the trend line only allows an indication of the tendency, but not an assessment of whether the points are on the safe side. On the other hand, the load-bearing capacities are compared with the absolute value of the standard as a function of the parameters examined. This evaluation can be used to assess whether the numerical results are on the safe side.

$$N_{1,\mathrm{Rd}} = C_\mathrm{f}\,\frac{f_{y0}t_0{}^2}{\sin\theta_1}\left(\frac{2\eta}{(1-\beta)\sin\theta_1}+\frac{4}{\sqrt{1-\beta}}\right)Q_\mathrm{f}/\gamma_{\mathrm{M5}} \tag{1}$$

$$Q_\mathrm{f} = (1-|n_0|)^{c_1} \quad \geq 0,4 \tag{2}$$

$$\text{for } n_0 < 0\,(\text{Compression}) : C_1 = 0,6 - 0,5\beta \tag{3}$$

$$\text{for } n_0 > 0\,(\text{Tension}) : C_1 = 0,1 \tag{4}$$

Steel grade

The steel grade resp. the yield strength has a linear influence on the joint load-bearing capacity $f(f_y) = f_y$ according to the design formulas for CFF (see Fig. 12a, red line). By adding the material factors C_f, this influence is reduced linearly depending on the steel grade (see Fig. 12a, dark red line). The trend line of the numerical results (dashed line) clearly shows the same slope as the red line with $f(f_y) = f_y$. The numerical results thus show a linear influence of the yield strength on the joint load-bearing capacity of axially stressed T-joints. In contrast, the dark red line shows a flatter slope due to the multiplication with a C_f factor. The evaluation in Fig. 12a shows the tendency that a reduction by a C_f factor is not required. The comparison of the absolute values (Fig. 12b) of the joint load-bearing capacities also shows that the influence of the yield strength is well represented by the normative design formula, but Fig. 12b also shows an overestimation of the joint load-bearing capacities for the β-ratio of $\beta = 0.8$.

Chord wall thickness t_0

The chord wall thickness t_0 has a quadratic influence on the joint load-bearing capacity $f(t_0) = t_0{}^2$ according to the normative design rules for CFF. Fig. 13a shows that the numerical results of the parameter study also demonstrate the quadratic influence of the wall thickness on the joint load-bearing capacity. From this it can be concluded that the analytical yield line model derived for the axially stressed T-joint also provides good agreement for the high-strength T-joints.

The evaluation of the absolute values, shown in Fig. 13b, also shows good agreement for β-ratios $\beta = 0.4$ and $\beta = 0.6$. For the large β-ratio ($\beta = 0.8$), the joint load-bearing capacities are overestimated by the normative design rules.

β-ratio

The evaluation of the influence of the β-ratio shows a large deviation of the numerical results from the normative design rules for large β-ratios (see Fig. 14a). The function for the influence of the β-ratio is described normatively by

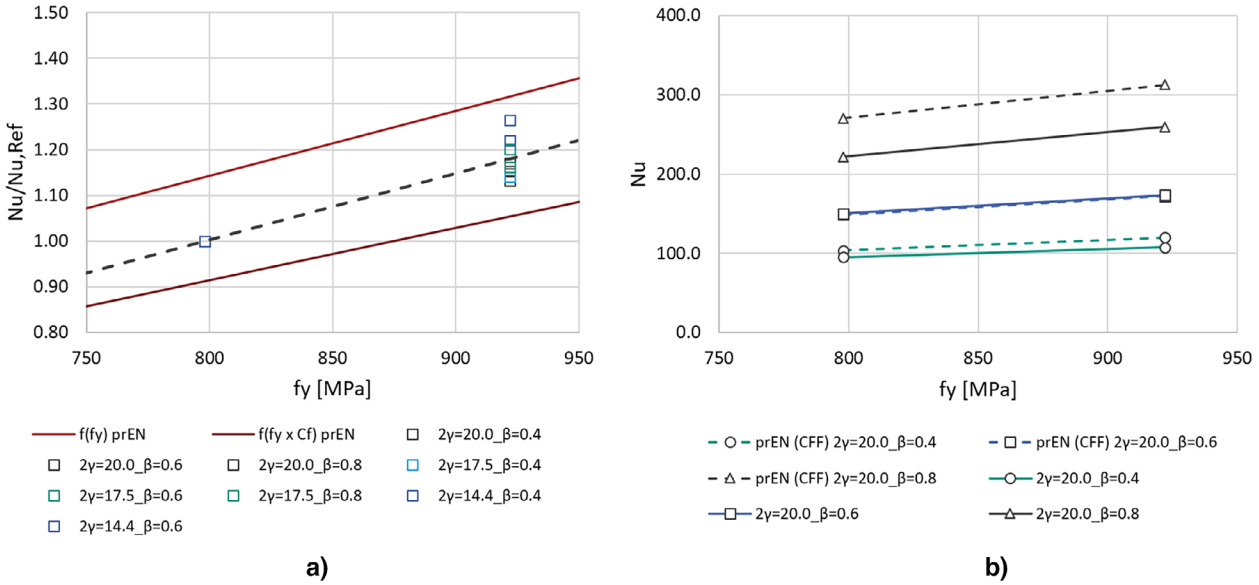

Fig. 12 Influence of the yield strength on the joint load-bearing capacity: a) reference value, b) absolute value

$f(\beta) = (2–\eta/(1–\beta)–\sin(\theta) + 4/(1–\beta)\,0.5)$. Above a β-ratio of $\beta = 0.7$, the trend line of the evaluated numerical joint load-bearing capacities shows a clear deviation from the line of the design formula function shown. By selecting a single-span beam support, the moment resistance of the chords is lower than the joint resistance according to the design rules of prEN 1993-1-8 [3]. The discrepancy described can also be seen in Fig. 14b based on the evaluation of the absolute values.

Degree of preload n_0

The results of the numerical parameter study in Fig. 15 show that the influence of the chord pre-stressing function (Eqs. (2)–(4)) is well represented in the design rules for a compression pre-tensioning of the chord up to 70 % chord utilisation. The evaluation in Fig. 15 shows that no reduction is required for a tensile preloading of the chord up to 70 % chord utilisation. However, this only applies to T-joints subjected to axial compression (compression–compression combination).

Weld dimension, a-dimension

The numerical validation of the experimental tests revealed a major influence of the weld dimension, more precisely the *a*-dimension of the weld. For this reason, the results of the parameter study already presented were generated on models without fillet weld, i.e., with a fully welded butt weld ($a = 0$). In order to be able to quantify the influence of the *a*-dimension, a parameter study was carried out for various *a*-dimensions of the weld.

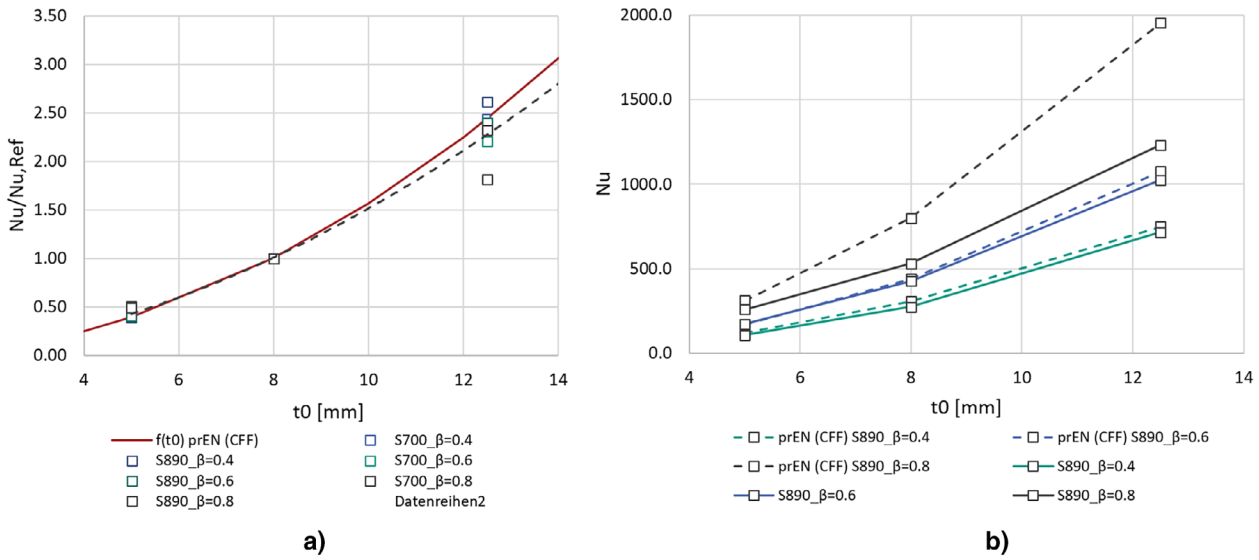

Fig. 13 Influence of the wall thickness of the chord on the joint load-bearing capacity: a) reference value, b) absolute value

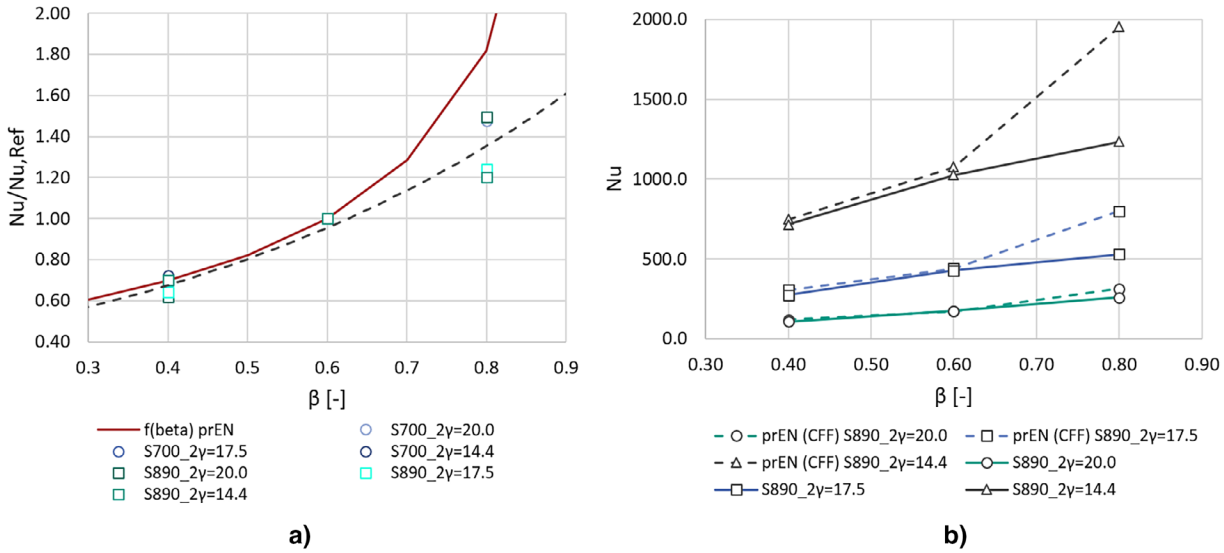

Fig. 14 Influence of the β-ratio on the joint load-bearing capacity: a) reference value, b) absolute value

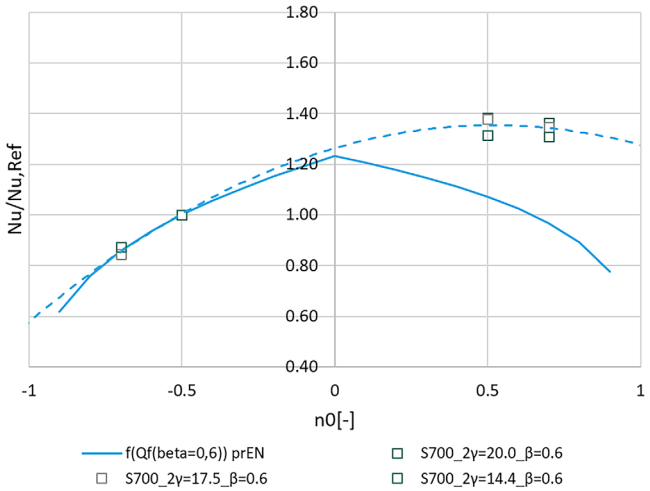

Fig. 15 Influence of chord utilisation on the joint load-bearing capacity

Tab. 3 Dimensions of the parameter study to analyse the influence of the fillet weld thickness ratio

Steel grade	2γ	β	b_0	b_1	a-dimension
S700MH	20	0.6	100 mm	60 mm	0–5 mm
S700MH	14.5	0.6	140 mm	84 mm	0–5 mm

The investigations were carried out on models using the material model for S700MH and the dimensions shown in Tab. 3.

Fig. 16a shows the influence of the a-dimension on the joint load-bearing capacity as a function of the absolute value of the a-dimension. An increase in the a-dimension always results in an increase of the joint resistance. This dependency is not included in the design formulas of prEN-1993-1-8 [3]. Since the two 2γ-ratios examined in the study have different brace dimensions, the percentage increases in joint load-bearing capacity differ between the two 2γ-ratios. However, if an effective β-ratio is calculated according to Eq. (5) and the increase in the joint load-bearing capacity is related to the increase in the β-ratio, it can be seen that the increase in the joint load-bearing capacity is independent of the 2γ-ratio and only depends on the increase in the β-ratio (see Fig. 16b). From an increase in the β-ratio by 10 %, a linear relationship between the ratio β_{eff}/β and the increase in joint load-bearing capacity can be seen.

$$\beta_{\text{eff}} = \frac{b_1 + 2 \cdot \sqrt{2} \cdot a}{b_0} \tag{5}$$

with:

β_{eff} effective width ratio;
a a-dimension; and
b_1,b_0 width of the brace and chord.

3.2 Bending-stressed T-joints

The diagrams shown in Fig. 17 represent the relationship between the numerically determined joint load-bearing capacity r_n and the nominal load-bearing capacity r_t using a C_f factor of 1.0. A distinction is made between the failure modes CFF and PSF for the steel grades S700MH (a) and S890QLH (b). In contrast to prEN 1993-1-8 [3], PSF was not calculated with a fictitious yield strength $0.8 \cdot f_u$ but with $1.0 \cdot f_y$. For S700MH, this results in a C_f factor of 0.96 – well above the value of 0.80 required in prEN 1993-1-8 [3]. The steel S890QLH achieves a C_f factor of 0.89, although

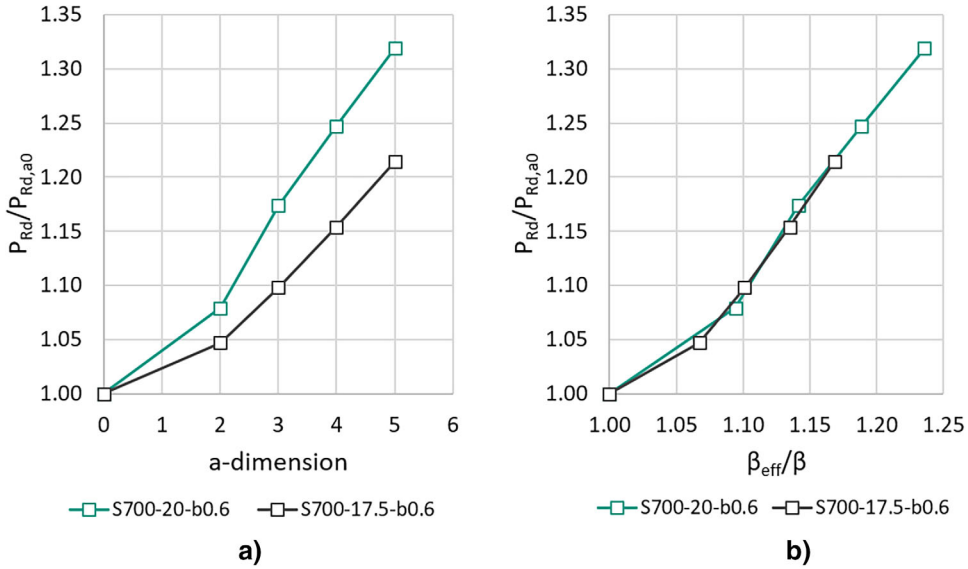

Fig. 16 Influence of the a) a-dimension and b) β_{eff}/β-ratio on the joint load-bearing capacity

further evaluations are necessary for reliable statements. The regressions shown in both diagrams are above the 45° line, which indicates a conservative design in accordance with prEN 1993-1-8 [3], especially for S700MH.

A detailed analysis of the available data shows that CFF is the dominant failure mode in the case of chord compressive pre-stressing, while PSF is the dominant failure mode in the case of chord tensile pre-stressing. In summary, it can be stated that tensile pre-stressing of the chord appears to have a positive influence on the C_f factor, even achieving a C_f factor $\geq$ 1.0. The present investigations show that the above statements are only valid for certain β-ratios between 0.4 and 0.7. This limitation must be considered when interpreting the results.

3.2.1 Influences on the load-bearing behaviour: bending

The analysis and evaluation of the results from the parameter study first require consideration of the composition of the resistance function for CFF mode, as defined in prEN 1993-1-8 [3]. To be able to analyse the influence of the chord pre-stressing on the load-bearing behaviour, the resistance function for CFF is considered in particular in the following since this function is dependent on the chord pre-stressing.

$$M_{ip,1,Rd} = C_f \cdot f_{y0} \cdot t_0^2 \cdot h_1 \cdot \left(\frac{1}{2\eta} + \frac{2}{\sqrt{1-\beta}} + \frac{\eta}{1-\beta}\right) \cdot Q_f/\gamma_{M5} \quad (6)$$

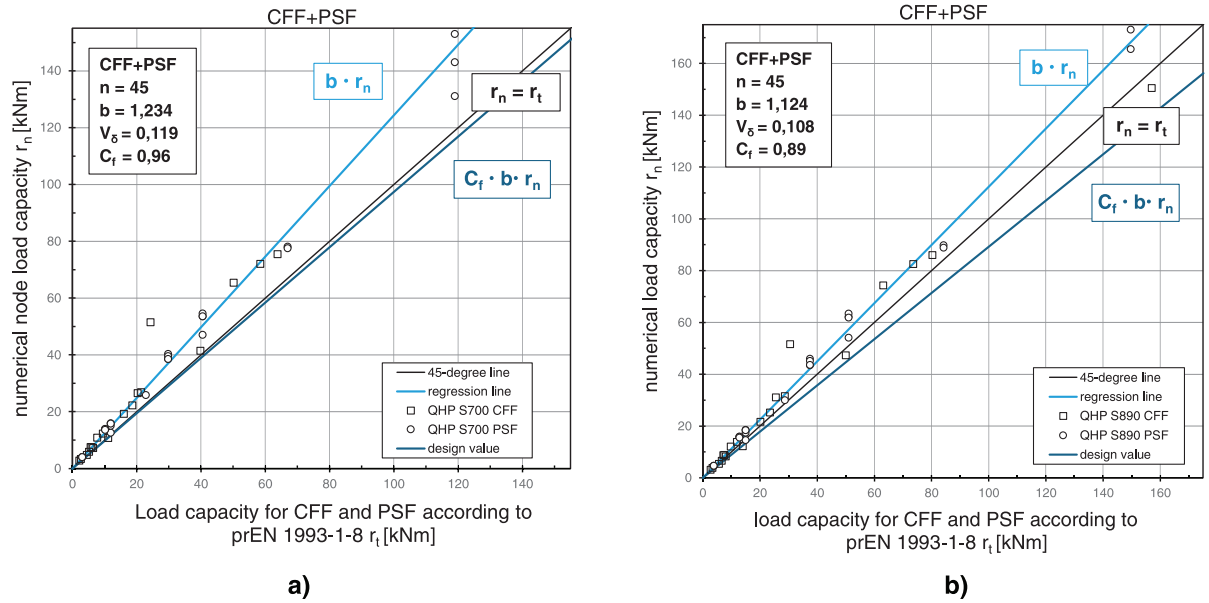

Fig. 17 Statistical analysis by material: a) S700MH and b) S890QLH

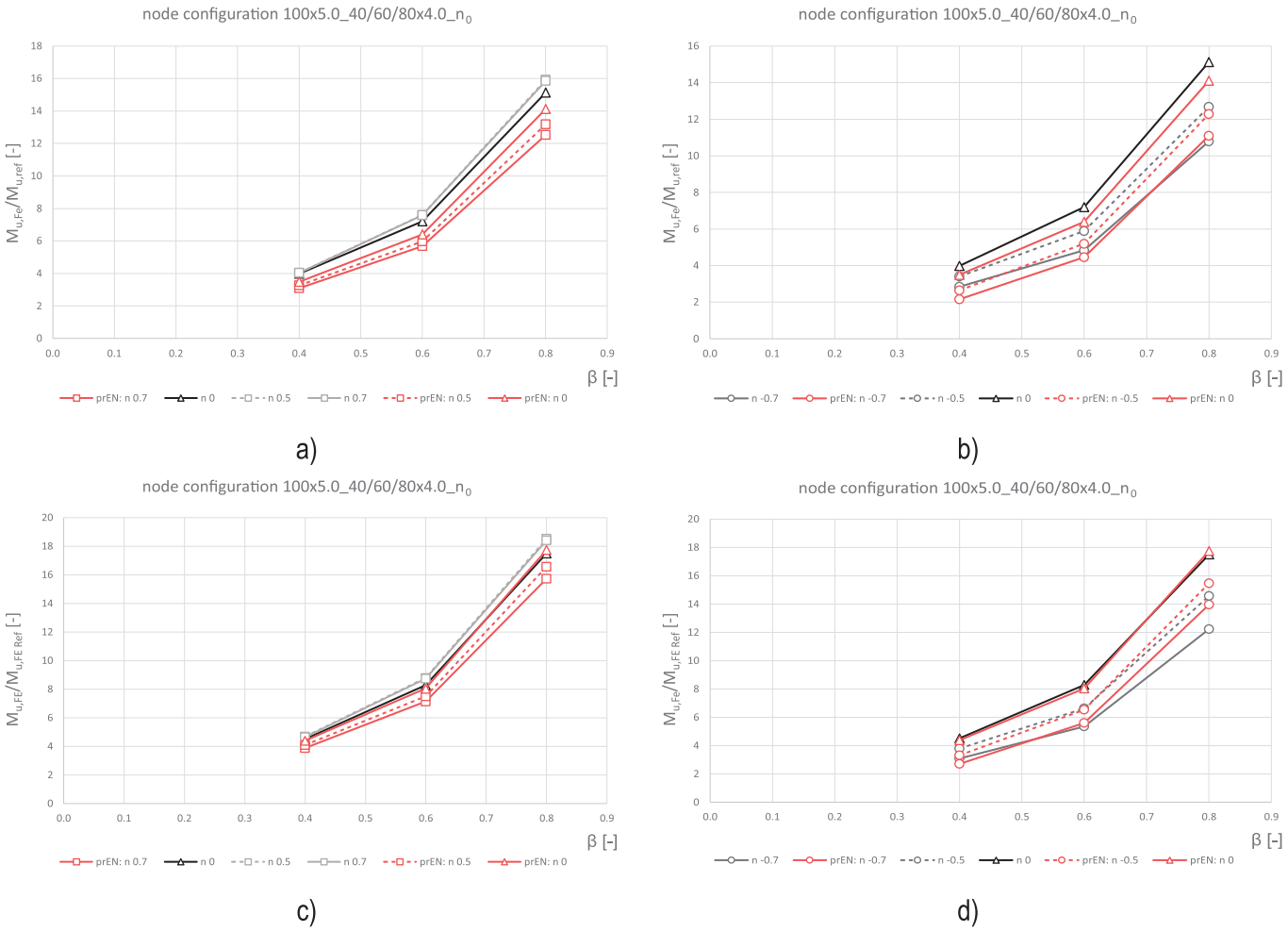

Fig. 18 Influence of the β-ratio: a) S700MH Compressive preload, b) S700MH Tensile preload, c) S890QLH Compressive preload, d) S890QLH Tensile preload

$$Q_f = (1 - |n_0|)^{c_1} \quad \geq 0,3 \tag{7}$$

$$\text{for } n_0 < 0 \text{ (Compression)}: \quad C_1 = 0,6 - 0,5\beta \tag{8}$$

$$\text{for } n_0 > 0 \text{ (Tension)}: C_1 = 0,1 \tag{9}$$

To enable a differentiated assessment of the influence of the various formula parameters, the formula was split up into its individual components and these were considered separately.

β-ratio

As shown in Fig. 18, the numerically determined moment resistance values are higher than the design values calculated according to prEN 1993-1-8 [3] for all tensile pre-stressed joint configurations. It was also found that a systematic underestimation of the numerical results by the corresponding design formulas according to the standard is also evident for compressive pre-stressing, especially for small β-ratios. This indicates the conservative nature of the design formulas according to the standard. For the material S890QLH, this tendency must be considered more detailed: for tensile pre-stressing, the numerical load-bearing capacities are only slightly above the standard values, whereas for compressive pre-stressing they exceed the numerical results to some extent.

Chord wall thickness t_0

The joint configuration $100 \times 5.0/8.0/12.5\_40 \times 4.0\_n_0$ of steel grade S700MH is considered in the following. It was investigated using three different chord wall thicknesses.

Fig. 19 shows that the parameter t_0, which is squared in the formula for CFF, only reflects reality to a limited extent. Up to $t_0 = 8.0$ mm, the standard-based function slightly underestimates the numerical results and therefore remains on the safe side. From $t_0 \geq 9.0$ mm, it significantly overestimates the load-bearing capacity. A check of the t_0 dependency is therefore recommended. The evaluations shown are limited exclusively to the material S700MH.

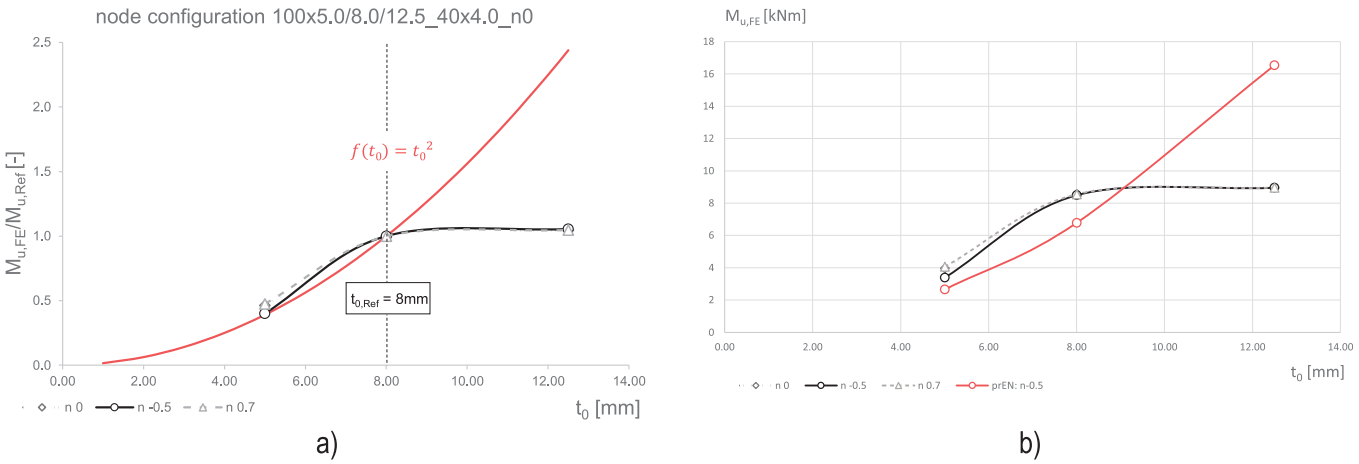

Fig. 19 Influence of chord thickness t_0: a) reference values $M_{u,FE}/M_{u,Ref}$ and b) absolute values $M_{u,FE}$ related to $t_{0,} = 8.0$ mm

Degree of preload n_0

The individual analysis of the chord member stress function as a function of the β-ratio shows a consistent curve in the compression range, which is supported by the numerical results. In the tensile load case, however, the function significantly reduces the joint load-bearing capacity, although the numerical values are significantly higher (see Fig. 20). Taking the above-mentioned aspects into account, it can be concluded that a horizontal course of the branch of the chord member tension function can be considered appropriate in the presence of chord tensile pre-stressing, as specified in the currently still valid standard DIN EN 1993-1-8 [20]. However, this statement only applies to a maximum tensile pre-stressing of 70 %, as the parameter study does not include any investigations into higher degrees of pre-stressing (see Fig. 20).

Comparable results were obtained for steel grade S890QLH (Fig. 20b). The existing statements on the chord member stress function therefore also apply. However, a revision of the chord member tension function is necessary for chord tensile pre-stressing, as the nominal reduction does not correspond to the numerical or experimental results and thus leads to an uneconomical design.

4 Conclusion

The numerical parameter studies for axial loaded T-joints prove that for β-ratios between $\beta = 0.4$–0.7, the failure mechanism CFF is well represented by the normative design rules. For the assessment, the decisive parameters yield strength f_y, β-ratio and chord wall thickness t_0 were considered individually. A comparison of the joint capacities given by the numerical results with the theoretical capacities according to prEN 1993-1-8 [3] shows that, even when using a C_f factor of 1.0, the results are still conservative. The parameter study shows a major influence of the weld dimension a on the load-bearing capacity of the T-joints. Increasing a increases the width ratio. This influence should be considered by introducing an effective width ratio β_{eff} in future. Further experimental and numerical parameter studies are necessary in order to be able to make a statement for β-ratios $\beta > 0.7$. The parameter study presented has shown that the joint load-bearing capacity is overestimated by the formulae of prEN

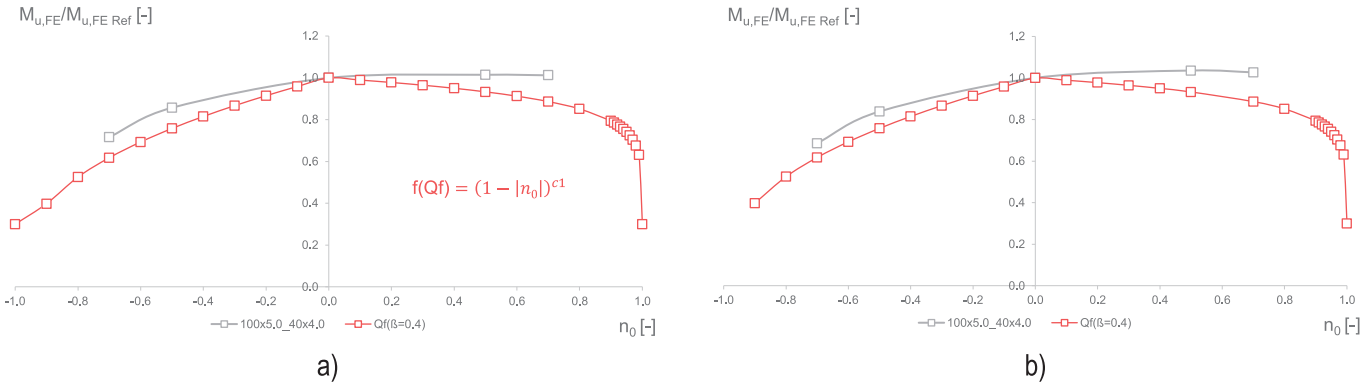

Fig. 20 Influence of the chord member load function in relation to the β-ratio: a) S700MH, joint configuration 100 × 5.0_40/60/80 × 4.0 and b) S890QLH, joint configuration 100 × 5.0_40/60/80 × 4.0

1993-1-8 [3] for large β-ratios. However, this fact may also be due to the peculiarity of the moment–normal force interaction of the T-joint. Further numerical investigations on an X-joint could be expedient.

The following conclusions could be drawn from the numerical parameter study for T-joints under bending with chord pre-stressing up to 70 % of the yield strength.

To correctly capture the influence of chord pre-stressing, a modification of the chord tension function appears possible. It can be deduced that a horizontal course of the branch of the chord tension function can be considered appropriate in the presence of chord tensile pre-stressing, as specified in the currently still valid standard DIN EN 1993-1-8 [20]. As the β-ratio increases, the chord tension function provides a more precise adjustment of the curve to the actual joint capacities. On the other hand, the influence of chord compressive pre-stressing tends to be considered correctly. However, the influence of the width ratio does not yet appear to be correctly respected.

The influence of chord pre-stressing on PSF should be further analysed. The calculation formula for the PSF does not currently appear to adequately describe the failure mode that occurs. The influence of the material strength and the width ratio must be further analysed and implemented. Using $1.0\times f_y$ in the PSF formula instead of using $0.8\times f_u$ could lead to more realistic and less conservative design results.

The analyses also show that the influence of the sheet thickness is overestimated in the design formula for CFF for sheet thicknesses t higher than 9 mm. The previous quadratic dependence on t_0 needs to be adjusted to enable a more precise description of the design resistance.

In summary, it can be stated that the Cf factor is currently on the safe side and prEN 1993-1-8 [3] can be assessed as conservative.

Acknowledgements

The research project ‘Static load-bearing behaviour of high-strength T-joints made of rectangular hollow sections under consideration of the chord preloading influence in steel construction, FOSTA research project P1504’ was funded by the Federal Ministry of Economic Affairs and Climate Action as part of the ‘Industrial Collective Research’ programme based on a resolution of the German Bundestag. This project IGF-Nr. 01IF21437N/P1504 from the Research Association for steel Application (FOSTA), Düsseldorf, was carried out at Karlsruhe Institute of Technology (KIT) and at the University of Applied Sciences Munich University of Applied Sciences Munich. The authors are grateful to the Research Association for Steel Application (FOSTA) for their financial support as well as all the industry partners for supplying materials and performing the welding work.

Open access funding enabled and organized by Projekt DEAL.

References

[1] DIN EN 10219-3:2020-11 (2020) *Kaltgeformte geschweißte Hohlprofile für den Stahlbau - Teil 3: Technische Lieferbedingungen für höher- und wetterfeste Stähle; Deutsche Fassung EN 10219-3:2020*. Berlin: Beuth Verlag GmbH.

[2] DIN EN 10210-3:2020-11 (2020) *Warmgefertigte Hohlprofile für den Stahlbau - Teil 3: Technische Lieferbedingungen für höher- und wetterfeste Stähle; Deutsche Fassung EN 10210-3:2020*. Berlin: Beuth Verlag GmbH.

[3] prEN 1993-1-8:2021-03 (2021) *Eurocode 3: Bemessung und Konstruktion von Stahlbauten - Teil 1-8: Bemessung von Anschlüssen; Deutsche und Englische Fassung prEN 1993-1-8:2021*. Berlin: Beuth Verlag GmbH.

[4] Ummenhofer, T. et al. (2024) *Static load-bearing behaviour of high-strength T-joints made of rectangular hollow sections under consideration of the chord preloading influence in steel construction, FOSTA research project P1504*. Düsseldorf: Forschungsvereinigung Stahlanwendung e.V. (FOSTA).

[5] Münch, A. et al. (2025) Experimental investigations of T-joints made of high-strength square hollow sections. Steel Construction 18, No. 3, pp. 180–193. https://doi.org/10.1002/stco.202500026

[6] Puthli, R. et al. (2010) *Adaption and extension of the valid design formulae for joints made of high-strength steels up to S690 for cold-formed and hot-rolled sections*. CIDECT Report 5BT-7/10.

[7] Fleischer, O. (2014) *Axial beanspruchte K-Knoten aus dünnwandigen Rechteckhohlprofilen* [Dissertation]. Karlsruher Institut für Technologie.

[8] Lu, L. H.; Winkel, G. D.; Yu, Y.; Wardenier, J. (1994) *Deformation limit for the ultimate strength of hollow section joints* in: Grundy, P.; Holgate, A.; Wong, B. [Eds.] *Tubular Structures VI: Proceedings of the 6th International Symposium on Tubular Structures*. Melbourne, Australia: Routledge.

[9] Münstermann, S. (2006) *Numerische Beschreibung des duktilen Schädigungsverhaltens von hochfesten Baustählen unter Berücksichtigung der Mikrostruktur* [Dissertation]. RWTH Aachen.

[10] Mayer, T.; Ringhand, D.; Barth, S. (2015) *Schädigungsvorhersage mit dem Johnson-Cook-Modell. Heilbronn*.

[11] Johnson, G. R.; Cook, W. (1985) *Fracture characteristics of three metals subjected to various strains, strain rates, temperatures and pressures*. Engineering Fracture Mechanics 21, No. 1, pp. 31–48.

[12] Engelhardt, I.; Ummenhofer, T.; Kuhlmann, U. (2024) *Hochfeste Hohlprofilfachwerke (Hochfeste Hohlprofilfachwerke)* in: Forschungsvorhaben HighTRUSS /FKZ Nr. 03TN0022. WIPANO.

[13] Voce, E. (1948) *The relationship between stress and strain for homogeneous deformations*. Journal of the Institute of Metals [online] 74, pp. 537–562. https://wbldb.lievers.net/10061146.html [accessed on: 03 Dec. 2024]

[14] Swift, H. W. (1952) *Plastic instability under plane stress*. Journal of the Mechanics and Physics of Solids 1, No. 1, pp. 1–18. https://doi.org/10.1016/0022-5096(52)90002-1

[15] Park, S.-J.; Lee, K.; Cerik, B. C.; Choung, J. (2019) *Ductile fracture prediction of EH36 grade steel based on Hosford–Coulomb model*. Ships and Offshore Structures 14, No. sup1, pp. 219–230. https://doi.org/10.1080/17445302.2019.1565300

[16] Yan, R.; Xin, H.; Veljkovic, M. (2021) *Ductile fracture simulation of cold-formed high strength steel using GTN damage model*. Journal of Constructional Steel Research184, No. 106832.

[17] Roth, C. C.; Mohr, D. (2016) *Ductile fracture experiments with locally proportional loading histories*. International Journal of Plasticity 79, pp. 328–354.

[18] DIN EN 10219-1:2006-07 (2006) *Kaltgefertigte geschweißte Hohlprofile für den Stahlbau aus unlegierten Baustählen und aus Feinkornnbaustählen - Teil 1: Technische Lieferbedingungen; Deutsche Fassung EN 10219-1:2006*. Berlin: Beuth Verlag GmbH.

[19] Hancock, J. W.; Mackenzie, A. C. (1976) *On the mechanisms of ductile failure in high-strength steels subjected to multi-axial stress-states*. Journal of the Mechanics and Physics of Solids 24, No. 2, pp. 147–160. https://doi.org/10.1016/0022-5096(76)90024-7

[20] DIN EN 1993-1-8:2010-12 (2010) *Eurocode 3: Bemessung und Konstruktion von Stahlbauten - Teil 1-8: Bemessung von Anschlüssen; Deutsche Fassung EN 1993-1-8:2005 + AC:2009*. Berlin: Beuth Verlag GmbH.

Authors

M. Eng. Pauline Markreiter (corresponding author)
pauline.markreiter@hm.edu
Institut für Material und Bauforschung
Hochschule München
Karlstr. 6
80333 München
Germany

Adrian Münch, M.Sc.
adrian.muench@kit.edu
Karlsruhe Institute of Technology
KIT Steel and Lightweight Structures
Otto-Ammann-Platz 1
76131 Karlsruhe
Germany

Prof. Dr.-Ing. Imke Engelhardt
Imke.engelhardt@hm.edu
Institut für Material und Bauforschung
Hochschule München
Karlstr. 6
80333 München
Germany

Dr.-Ing. Philipp Weidner
philipp.weidner@kit.edu
Karlsruhe Institute of Technology
KIT Steel and Lightweight Structures
Otto-Ammann-Platz 1
76131 Karlsruhe
Germany

Prof. Dr.-Ing. Thomas Ummenhofer
thomas.ummenhofer@kit.edu
Karlsruhe Institute of Technology
KIT Steel and Lightweight Structures
Otto-Ammann-Platz 1
76131 Karlsruhe
Germany

How to Cite this Paper

Markreiter, P.; Münch, A.; Engelhardt, I.; Weidner, P.; Ummenhofer, T. (2025) *Numerical investigations of T-joints made of high-strength square hollow sections*. Steel Construction 18, No. 3, pp. 194–208.
https://doi.org/10.1002/stco.202500025

This paper has been peer reviewed. Submitted: 24. June 2025; accepted: 10. July 2025.